Journal of Cancer Research and Experimental Oncology Vol. 3(7), pp. 76-83, October 2011
Available online at http://www.academicjournals.org/JCREO
ISSN 2141-2243 ©2011 Academic Journals

Full Length Research Paper

Preliminary analysis of radiation dose effects to rat femora microstructure using synchrotron radiation computed microtomography

Liebert Parreiras Nogueira[1]*, Christiano Jorge Gomes Pinheiro[2], Regina Cély Barroso[2], Delson Braz[1], Carlos Eduardo de Almeida[3], Cherley Borba Andrade[3] and Giuliana Tromba[4]

[1]Nuclear Instrumentation Laboratory / COPPE / UFRJ, P.O. Box 68509, 21945-970, Rio de Janeiro, Brazil.
[2]Physics Institute / State University of Rio de Janeiro, 20550-900, Rio de Janeiro, Brazil.
[3]Laboratory of Radiological Sciences / State University of Rio de Janeiro, Rio de Janeiro, Brazil.
[4]Sincrotrone Trieste SCpA, Strada Statale S.S. 14 km 163.5, 34012 Basovizza, Trieste, Italy.

Accepted 9 September, 2011

In this work we investigated the consequences of irradiation in the femur of rats to a radiation dose of 5 Gy. Three different sites in femur specimens were imaged using synchrotron radiation microcomputed tomography to assess trabecular bone microarchitecture: head, distal metaphysis and distal epiphysis. Histomorphometric quantification was extracted directly from the 3D tomographic images using synchrontron radiation. The 3D tomographic images were obtained at the SYnchrotron Radiation for MEdical Physics (SYRMEP) beamline at the Elettra Synchrotron Laboratory in Trieste, Italy. A better understanding of the biological interactions that occur after exposure to photon radiation is needed in order to optimize therapeutic regimens and facilitate development and strategies that decrease radiation-induced side effects in humans. Results showed significant differences between irradiated and non-irradiated mostly in head and distal metaphysis bone sites.

Key words: Radiotherapy, microtomography, synchrotron radiation, dose effects, histomorphometry, bone microstructure.

INTRODUCTION

Therapeutic doses of radiation may also have deleterious consequences on bone health (Hall and Giaccia, 2000). In clinical practice, the quantitative evaluation of bone tissue relies on measurements of bone mineral density values, which are closely associated with the risk of osteoporotic fracture (Sone et al., 2004). Improved survival rates of cancer patients receiving radiotherapy increase the interest to understand the mechanisms and long-term effects of radiation-induced bone loss.

Although bone strength is mainly determined by bone mineral density, the crucial role of trabecular bone architecture for predicting fracture risk has been proven in recent years. Acknowledging the importance of trabecular bone microstructure, new tools that allow a three-dimensional (3D) non-invasive investigation of the bone microstructure and a quantitative analysis of trabecular architecture have been developed (Odgaard, 1997).

X-ray microtomography (μCT) is a non-destructive technique, which enables investigation of the three-dimensional structure of an object at the micron scale. Experimentally, a series of digital radiographies at different angular positions of the sample is recorded and the reconstruction of the slice, which represents a virtual thin-section of the sample, is obtained by using mathematical procedure such as filtered back projection (Uesugi et al., 2006).

The Synchrotron radiation (SR) combined with μCT (SR-μCT) is a very useful technique when it comes to three-dimensional (3D) imaging of complex internal structures. The μCT experiments presented in this paper were conducted at the third generation Elettra Synchrotron Light Laboratory in Trieste (Italy). Some

*Corresponding author. E-mail: liebertrj@gmail.com. Tel: +5521 2334-0699.

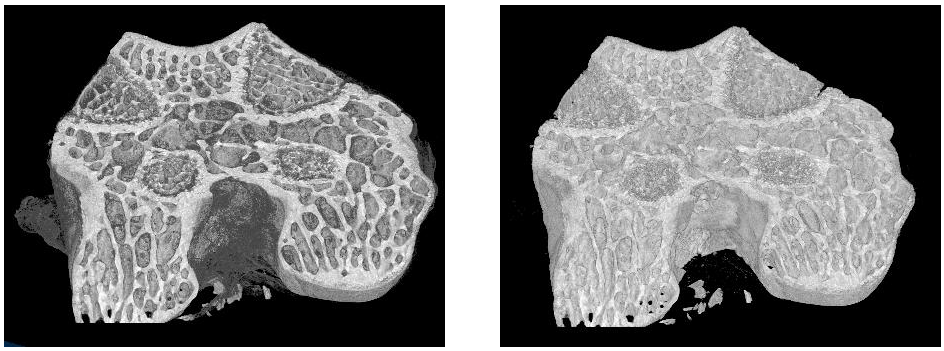

a b

Figure 1. (a) 3D image showing soft tissue and marrow attached to the bone and (b) respective 3D image after complete segmentation.

peculiar aspects of this kind of sources for X-ray imaging are introduced. These aspects are associated to the high energy and low emittance of the electron beam. This allows to study heavy or bulky samples in transmission geometry, and to perform *in-situ* or real-time (at the temporal scale of about 0.1 s) experiments. In recent years, synchrotron radiation micro-computed tomography (SR-μCT) has been applied as a nondestructive, high spatial resolution method to image and quantify the trabecular microarchitecture (Martín-Badosa et al., 2003).

The histomorphometric analysis tries to relate values obtained from the images with the 3D structure of the sample. To assess bone microarchitecture, 3D stereological indices are extracted according to the standard definitions used in histomorphometry: bone volume (BV), bone surface (BS), bone volume to total volume (BV/TV), surface to volume of the sample (BS/BV), connection thickness (Tb.Th), connection number (Tb.N) and connection separation (Tb.Sp) (Nogueira et al., 2010; Oliveira and Lopes, 2004; Chappard et al., 2008)

Many diseases, which lead to alterations in bone microarchitecture, have already been investigated by means of μCT histomorphometric quantification. Akhter et al. (2007) studied changes in bone structure pre and post-menopause using 3D-μCT histomorphometry by evaluating BV/TV, Tb.Th, Tb.Sp, Tb.N and some other parameters. Alterations in all the parameters were reported. Sone et al. (2004) compared trabecular bone microarchitecture and degree of mineralization between osteoblastic bone metastasis and degenerative osteosclerosis using synchrotron radiation μCT. Their results showed significant changes in some analyzed parameters (BV/TV and Tb.N) while no difference was noticed in Others (Tb.Th and BS/BV). Chappard et al. (2006) evaluated microarchitectural alterations in osteoarthritic bones using synchrotron 3D-μCT histomorphometry, and all morphological parameters showed differences between osteoarthritis and osteoporosis samples. Patel et al. (2003) analyzed variation in trabecular bone structure in different compartments and depths of the knee using 3D-μCT histomorphometry, and showed that the parameters vary with the depth from knee. Boyd et al. (2006) evaluated bone morphometric parameters variation in ovariectomized rats with *in vivo* μCT, during a certain period of time. They found significant changes in morphological indices by longitudinal analysis of the rats.

In this work, a home-made software routine developed by the Medical Physics Group at the Physics Institute of the State University of Rio de Janeiro was used to compute these parameters. A better understanding of the biological interactions that occur after exposure to photon radiation is needed in order to optimize therapeutic regimens and facilitate development and strategies that decrease radiation-induced side effects. In this framework, this work aims to use three-dimensional SR-μCT to investigate the dose effects of photon irradiation on bone microarchitecture.

METHODOLOGY

Samples

Wistar rats were obtained from the Laboratory of Radiological Sciences of State University of Rio de Janeiro, Brazil. The study was approved by the research and ethical committee of the State University of Rio de Janeiro. The animals were maintained under standard animal facility condition. Two adult female Wistar rats were exposed to a sublethal radiation dose of 5 Gy applied to the abdominopelvic field following anesthesia, using a small radiation field size generated by a ^{60}Co source 75 cm away from the skin. After 3 days, the femora were excised and immediately fixed with 10% formaldehyde neutral buffered solution. The specimens were carefully cleaned of non-osseous tissues and were allowed to air dry. Although adjacent tissues were removed, some tissue still remained stuck to the bone. In the case of computed microtomography it is not of great concern as the remaining soft tissue and the marrow can be easily removed at the time of image segmentation, just as it is shown in Figure 1. For control specimens, the same cleaning procedure was performed.

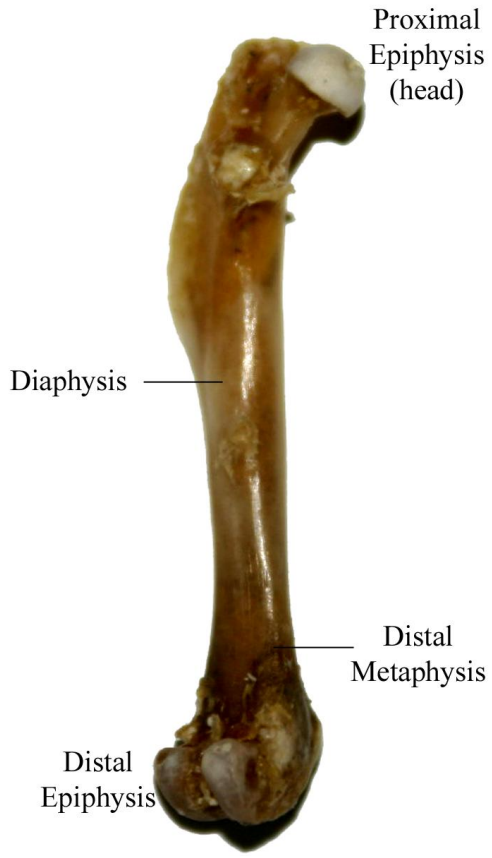

Figure 2. Selected sites of a typical femur specimen to be analyzed.

Three regions of interest were selected so that histomorphometric indices could be calculated from the trabecular bones at the following sites: proximal epiphysis (head), distal epiphysis and distal metaphysis as shown in Figure 2. In each region of interest, four different sites were evaluated so that statistic relevance could be achieved.

Experimental setup

All experiments were performed using the tomographic setup on SYnchrotron Radiation for MEdical Physics (SYRMEP) beamline at the Elettra Synchrotron Laboratory in Trieste, Italy. The setup has precise alignment of the rotation axis of the sample with the detector pixels. The beamline provides, at a distance of about 23 m from the source, a monochromatic laminar section X-ray beam with a maximum area of about 160 × 5 mm^2 at 20 keV. The monochromator, that covers the entire angular acceptance of the beamline, is based on a double Si(111) crystal system working in Bragg configuration (Abrami et al., 2005).

Microtomography consists of recording a large number of radiographs (projections) for each sample. In this work 900 projections were acquired while the sample was rotated stepwise over 180 degrees in 0.2 degree steps. A micrometric vertical and horizontal translation stage allows the positioning and the scanning of the sample with respect to the stationary beam and a rotational stage, with a resolution of 0.001° allows the acquisition of the projections. High-resolution images were obtained by means of a 16-bit CCD (Charge Coupled Device) camera, 2048×2048 pixels, 14 µm pixel size (maximum spatial resolution: 25 µm). The energy was set to 21 keV. The exposure time was about 2.7 s per projections. Dark current and reference images without sample were recorded to perform flat field correction on the projections. Figure 3 presents the setup and the main components used in this experiment.

Histomorphometric evaluation

The 3D reconstructed data are a collection of coefficients distributed regularly into the space. The 3D tomography yields all the spatial information needed to evaluate the parameters BV/TV and BS/BV directly from the volume. A region of interest (ROI) was defined containing only trabecular bone. After the definition of the ROI, bone should be separated from background. Figure 4 shows the gray-level histogram for one of the samples, showing clearly two well-differentiated peaks, corresponding to background and bone. Image segmentation is a critical issue in image processing and to date, no standard segmentation method has been developed for trabecular bone images. The threshold value is very important to correctly evaluating the proposed (Hara et al., 2002). In this work, automatic segmentation based on an iterative selection method (Riddler and Calvard, 1978) was used to distinguish bone and background, so that histomorphometric quantification could be performed.

Histomorphometric analysis tries to relate values obtained from the images with the 3D structure of the sample. The first method adapting the conventional procedure of histomorphometry to digital images was first presented by Feldkamp et al. (1989). For conventional technique, which entails substantial preparation of the specimen, sectioning and manual quantification, all parameters are evaluated from slices. The 3D histomorphometry is more compatible with the morphologic parameters: volume and surface. The obtained results reveal the potentials in using 3D tomographies to extract and evaluate histomorphometric parameters compared to 2D analysis since it avoids extrapolations (Oliveira and Lopes, 2004).

The quantitative assessment was performed using a home-made software which uses a voxel representation of the volume of microstructure (Oliveira et al., 2003). The total volume (TV) is the number of voxels contained on the volume data file. The total surface and the volume of the microstructure are counted summing the areas and volumes of each individual model found in the data volume. From the total surface (BS) and the total sample volume (BV), the other parameters can be calculated (Nogueira et al., 2010). This approach is based on Parffit's principles of the "plate and rod" model (Chappard et al., 2008).

$$Tb.Th = \frac{2BV}{BS} \quad (1)$$

$$Tb.N = \frac{BS}{2TV} \quad (2)$$

$$Tb.Sp = \frac{2(TV - BV)}{BS} \quad (3)$$

RESULTS AND DISCUSSION

The tomographies were reconstructed on one slice at a time with the Syrmep Tomo-Project software (Montanari,

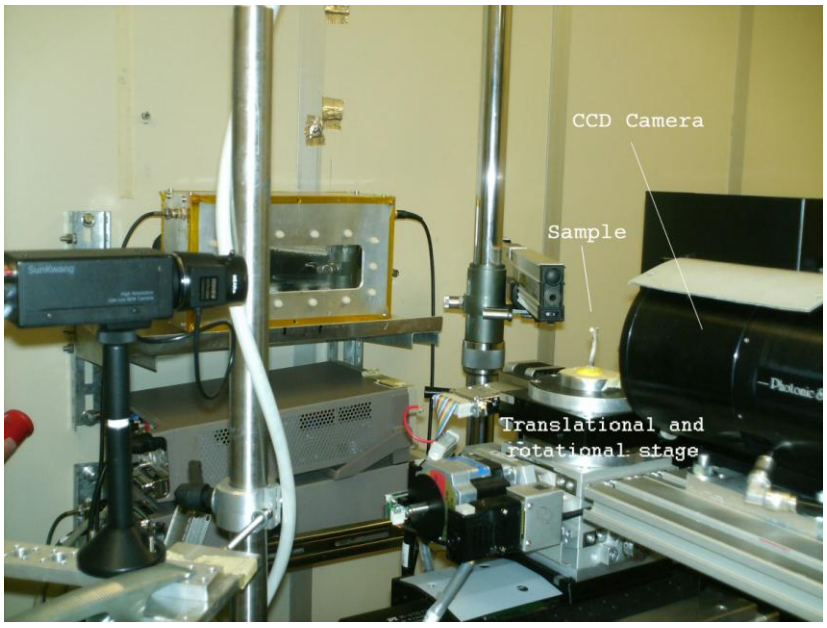

Figure 3. Experimental setup at the SYEMEP beamline.

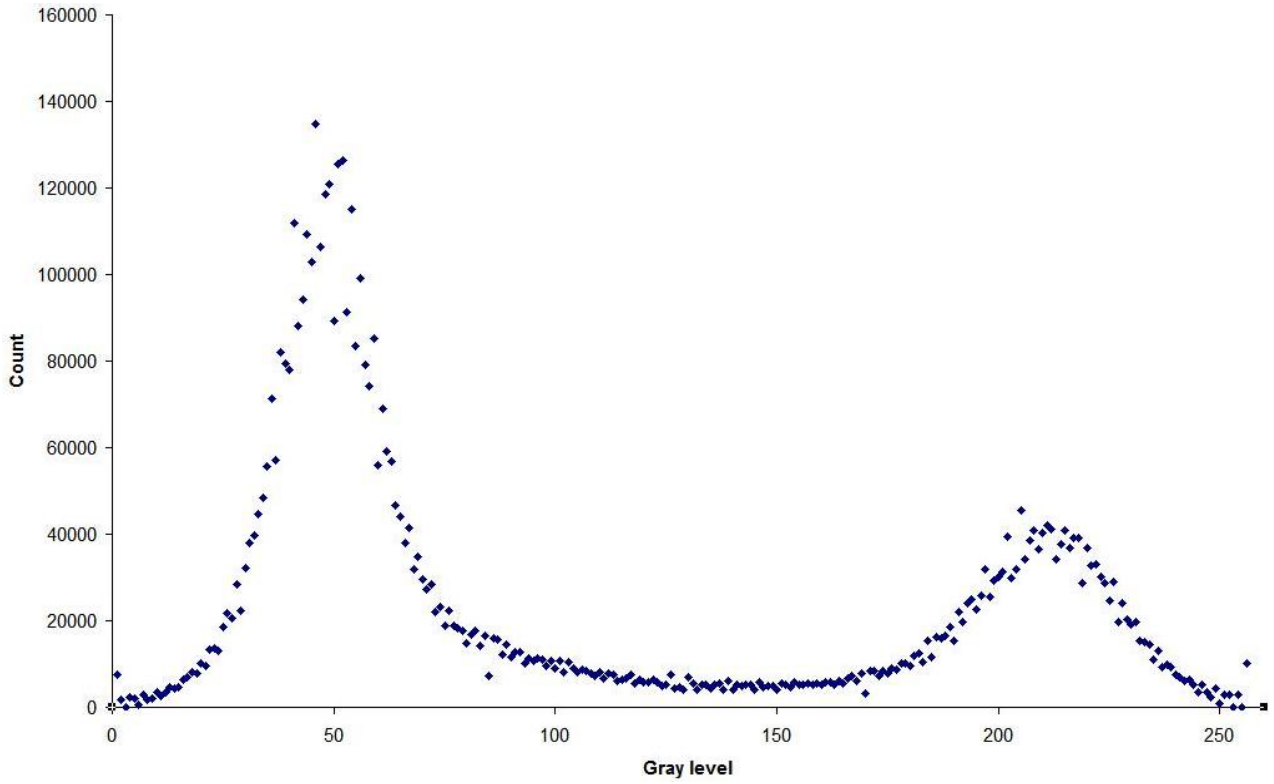

Figure 4. Gray level histogram.

2003) written in interactive data language (IDL), using a filtered back projection algorithm to retrieve the 3D bone structure image.

A long bone such as the femur consists of a centre piece, the shaft (diaphysis) and a thickened head (epiphysis) at each end: proximal epiphysis (closer to point of attachment) and distal epiphysis (farther from point of attachment). The intermediate regions between

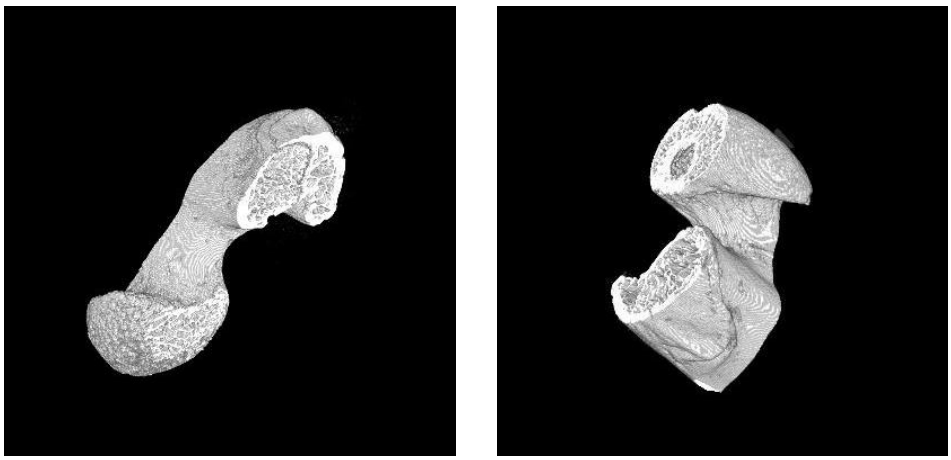

Figure 5. 3D rendering of proximal epiphysis (head): (a) Control and (b) irradiated specimens.

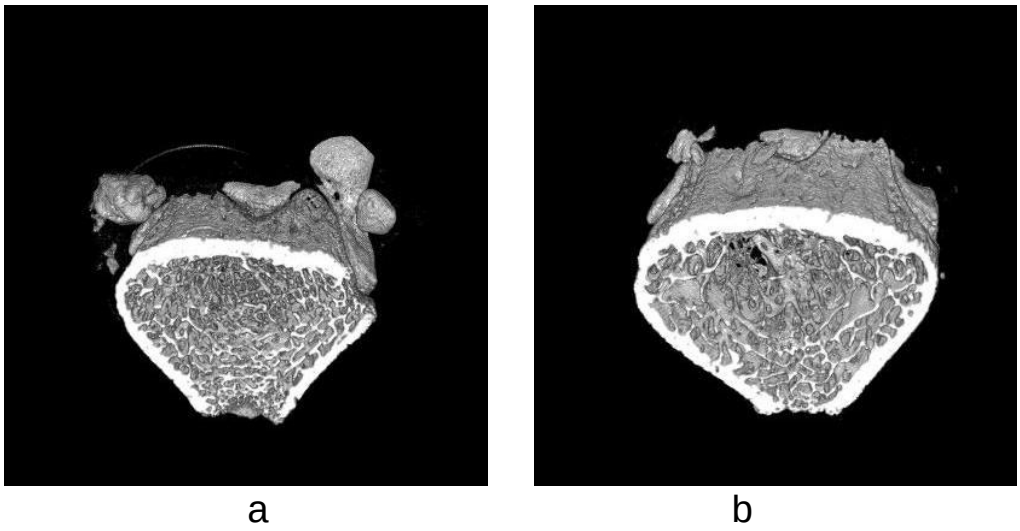

Figure 6. 3D rendering of distal metaphysis: (a) Control and (b) irradiated specimens.

the diaphysis and the epiphyses are called metaphyses. The diaphysis consists mostly of strong, dense bone called compact bone and houses marrow (medullary) cavity, which mostly stores yellow (fatty) marrow. As the diaphysis is mainly composed of cortical bone, it was not included on the quantification analysis. The samples were imaged in three different regions: proximal epiphysis (head), distal metaphysis and distal epiphysis.

Five morphological parameters were examined: bone volume fraction (BV/TV), bone surface-to-volume ratio (BS/BV), obtained directly from the images (primary parameters), trabecular number (Tb.N), trabecular thickness (Tb.Th) and trabecular separation (Tb.Sp), calculated indirectly from the primary parameters.

The reconstructed slices can be visualized as stacks of 2D images. 3D views of the sample can also be obtained by volume rendering procedures. 3D µCT images of the assessed samples are presented in Figures 5 to 7.

Within the head site, no significant difference was found between BV/TV of both groups (Figure 8). However, significant difference was found between BS/BV (-25.6%), Tb.Th (33.9%), Tb.N (-23.1%) and Tb.Sp (26.6%) of the groups. The decrease in BS/BV suggests that the irradiated femur site is less fragmented than the non-irradiated one. Changes in BV/TV after radiotherapy treatment has also been reported in literature (Zhang et al., 2010; Chen et al., 2002; Hopewell, 2003) and no significant alteration was found as well.

BV/TV and Tb.N decreased (-16.8 and -24.5%

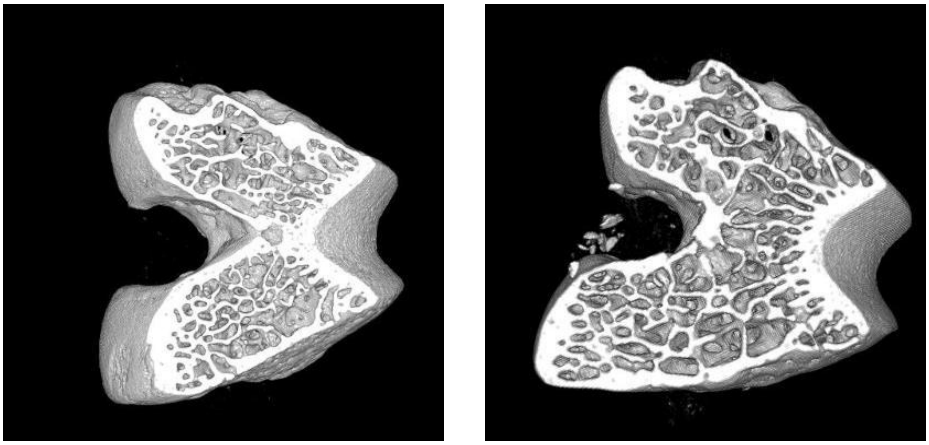

Figure 7. 3D rendering of distal epiphysis: (a) Control and (b) irradiated specimens.

respectively) in the irradiated distal metaphysis relative to the control one, while Tb.Sp increased (40.8%) significantly. Otherwise no important difference was observed on BS/BV and Tb.Th parameters at this same site. These data are consistent with a recent study including the same femur site (Willey et al., 2010). At the distal epiphysis site, no significant difference was observed in any parameter between the irradiated and control groups.

Irradiation induced a mild increase in trabecular thickness in all femur sites. Other studies also presented this alteration, in other animal models (Sawajiri et al., 2003).

Conclusions

In this present study, the assessment of bone microarchitecture using SR-μCT was performed and the resulting images showed excellent resolution, mainly due to monochromatic characteristics of the beam (non beam hardening effects) and the parallel geometry (less approximation in the reconstruction algorithms) which are key points for an accurate binarization (Landis and Keane, 2010). SR-μCT proved to be a very powerful tool as alternative for investigating bone microarchitecture in post-irradiated specimens. SR-μCT provides information about internal structure with a 3D visualization alternative, besides providing quantitative analyses.

These preliminary results showed some differences between irradiated and non-irradiated in head and distal metaphysis sites, while no significant difference was observed at the distal epiphysis. The most noticeable change was in the distal metaphysis, which presented a significant decrease on BV/TV. The relative bone loss (decreased BV/TV) between irradiated and non-irradiated femora in the distal metaphysis site accompanied by lower Tb.N and higher Tb.Sp with little or no change in Tb.N seems to indicate that radiation-induced bone loss is manifested through decreased connectivity and loss of thin trabecular elements. It has already been reported that radiotherapy produces an environment of hypoxia, hypovascularity, and hypocellularity in local tissues. Therefore apoptosis of osteoblasts, osteocytes, osteoprogenitor cells, and endothelial cells occurs after radiotherapy, which leads to progressive hyalinization and fibrosis of medullary spaces and, subsequently, to reduction of osseous vascularization (Blanco and Chao, 2006). All this leads to alterations on the balance of osteoblasts and osteoclasts and thus, changes in bone formation, what can explain the preliminary results found in our work.

Although these results suggest radiation-induced effects in bone microarchitecture, the number of testing samples is still low. Validations on a higher and totally independent set of samples are being conducted and this forms the basis of our ongoing studies. The precise mechanisms of radiation-induced bone loss are still unclear, although radiation induced effects on bone cells have already been observed at high dose levels (Gal et al., 2000; Scheven et al., 1987). Further studies addressing this issue, which make use of standard techniques like histology are on the way to complement this work, as well as analysis of bone of rats which underwent chemotherapy treatment as adjuvant to radiotherapy.

ACKNOWLEDGEMENTS

The authors thank the Brazilian agencies Conselho Nacional de Desenvolvimento Científico e Tecnológico (CNPq) and Fundação de Amparo à Pesquisa do Estado do Rio de Janeiro (FAPERJ) for financial support. This

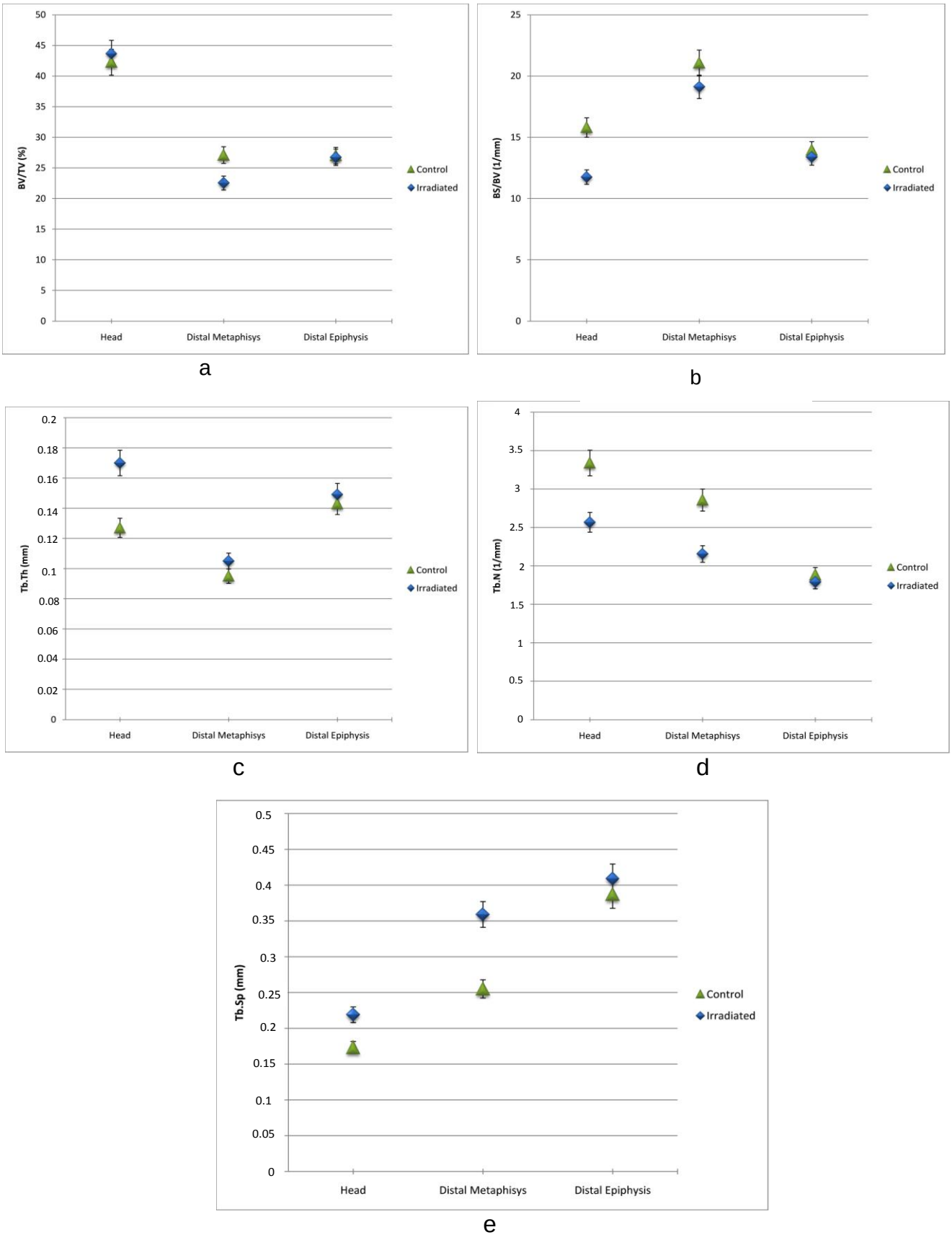

Figure 8. Histomorphometric parameters for the control and irradiated specimens in the different femur sites.

work was supported by ICTP-ELETTRA Users Programme (Project 2007834). We acknowledge the SYRMEP group, particularly Franco Zanini and Diego Dreossi for help during image acquisition and reconstruction.

REFERENCES

Abrami A, Arfelli F, Barroso RC, Bergamaschi A, Billè F, Bregant P, Brizzi F, Casarin K, Castelli E, Chenda V, Dalla Palma L, Dreossi D, Fava C, Longo R, Mancini L, Menk R-H, Montanari F, Olivo A, Pani S, Pillon A, Quai E, Ren Kaiser S, Rigon L, Rokvic T, Zanetti A, Zanini F (2005). Medical applications of synchrotron radiation at the SYRMEP beamline of ELETTRA. Nucl. Instrum. Meth. A., 548: 221-227.

Akhter MP, Lappe JM, Davies KM, Recker RR (2007). Transmenopausal changes in trabecular bone structure. Bone, 41: 111-116.

Blanco AI, Chao C (2006). Management of radiation-induced head and neck injury, Cancer Treat. Res., 128: 23-41.

Boyd SK, Davison P, Müller R, Gasser JA (2006). Monitoring individual morphological changes over time in ovariectomized rats by *in vivo* micro-computed tomography. Bone, 39(4): 854-862.

Chappard C, Peyrin F, Bonnassie A, Lemineur G, Brunet-Imbault B, Lespessailles E, Benhamou CL (2006). Subchondral bone micro-architectural alterations in osteoarthritis: A synchrotron micro-computed tomography study. Osteoarthr. Cartil., 14: 215-223.

Chappard D, Baslé M-F, Legrand E, Audran M (2008). Trabecular bone microarchitecture: The microarchitecture of trabecular bone: A Rev., Morphol., 92: 162-170.

Chen HHW, Lee B-F, Guo HR, Su W-R, Chiu N-T (2002). Changes in bone mineral density of lumbar spine after pelvic radiotherapy, Radiother. Oncol., 62: 139-242.

Feldkamp LA, Goldstein SA, Parfitt AM, Jesion G, Kleerekoper M (1989). The direct examination of 3-dimensional bone architecture invitro by computed-tomography, J. Bone Miner. Res., 4: 3-11.

Gal TJ, Munoz-Antonia T, Muro-Cacho CA, Klotch DW (2000). Radiation Effects on Osteoblasts *in vitro*: A Potential Role in Osteoradionecrosis. Arch. Otolaryngol. Head Neck Surg., 126: 1124-1128.

Hall EJ, Giaccia AJ (2000). Radiobiology for the Radiologist, third ed., Lippincott Williams & Wilkins, Philadelphia.

Hara T, Tanck E, Homminga J, Huiskes R (2002). Variations on the assessment of structural and mechanical trabecular bone properties. Bone, 31(1): 107-109.

Hopewell JW (2003). Radiation-therapy effects on bone density. Med. Pediatr. Oncol., 41: 208-211.

Landis EN, Keane DT (2010). X-ray microtomography. Mater. Characterization, 61: 1305-1316.

Martín-Badosa E, Amblard D, Nuzzo S, Elmoutaouakkil A, Vico L, Peyrin F (2003). Excised Bone Structures in Mice: Imaging at Three-dimensional Synchrotron Radiation Micro CT. Radiol., 229: 921-928.

Montanari F (2003). SYRMEP TOMO Project, tutorial. (www.ts.infn.it/experiments/ syrma/SYRMEP).

Nogueira LP, Braz D, Barroso RC, Oliveira LF, Pinheiro CJG, Dreossi D, Tromba G (2010). 3D histomorphometric quantification of trabecular bones by computed microtomography using synchrotron radiation. Micron, 41: 990-996.

Odgaard A (1997). Three-dimensional methods for quantification of cancellous bone architecture. Bone, 20: 315-328.

Oliveira LF, Lopes RT (2004). 3D Hismorphometric Quantification From 3D Computed Tomography, Nucl. Instrum. Meth. A., 525: 406-411.

Oliveira LF, Lopes RT, Jesus EFO, Braz D (2003). 3D X-ray tomography to evaluate volumetric objects. Nucl. Instrum. Meth. A., 505: 573-576.

Patel V, Issever AS, Burghardt A, Laib A, Ries M, Majumdar S (2003). MicroCT evaluation of normal and osteoarthritic bone structure in human knee specimens, J. Orthop. Res., 21(1): 6-13.

Riddler TW, Calvard S (1978). Picture thresholding using an iterative selection method. IEEE Trans. Syst. Man Cybernet. SMC., 8: 630-632.

Sawajiri M, Mizoe J (2003). Changes in bone volume after irradiation with carbon ions. Radiat. Environ. Biophys., 42: 101-106.

Scheven BA, Wassenaar AM, Kawilarang-de Haas EW, Nijweide PJ (1987). Direct and indirect radiation effects on osteoclast formation *in vitro*. Bone Miner., 4: 291-300.

Sone T, Tamada T, Jo Y, Miyoshi H, Fukunaga M (2004). Analysis of three-dimensional microarchitecture and degree of mineralization in bone metastases from prostate cancer using synchrotron microcomputed tomography. Bone, 35: 432-438.

Uesugi K, Sera T, Yagi N (2006). Fast tomography using quasi-monochromatic undulator radiation. J. Synchrotron Rad., 13: 403-407.

Willey JS, Livingston EW, Robbins ME, Bourland JD, Tirado-Lee L, Smith-Sielicki H, Bateman TA (2010). Risedronate prevents early radiation-induced osteoporosis in mice at multiple skeletal locations. Bone, 46: 101-111.

Zhang WB, Zheng LW, Chua D, Cheung LK (2010). Bone regeneration after radiotherapy in an animal model. J. Oral Maxillofac. Surg., 68: 2802-2809.